*Thermochimica Acta*, 155 (1989) 187–202
Elsevier Science Publishers B.V., Amsterdam – Printed in The Netherlands



# ISOTHERMAL AND NON-ISOTHERMAL CRYSTALLIZATION DURING WARMING IN AQUEOUS SOLUTIONS OF 1,3-BUTANEDIOL: COMPARISON OF CALORIMETRY AND CRYOMICROSCOPY

PATRICK MEHL

*Transplantation Laboratory, The Holland Laboratory for Research and Development, American Red Cross, 15601 Crabbs Branch Way, Rockville, MD 20855 (U.S.A.)*

(Received 28 March 1989)

## ABSTRACT

Preservation by low temperature vitrification is being developed for the cryopreservation of mammalian organs. The purpose is to avoid ice crystallization, which can cause damage during cooling or warming. With the high cryoprotectant concentrations being used, crystallization is easily avoided during cooling, but not during rewarming at practical warming rates. Assessment of the amount of crystallization occurring during warming is therefore necessary.

1,3-butanediol is a good glass-former and a good cryoprotectant for red blood cells. Similar to 1,2-propanediol, it has already been used for the vitrification of erythrocytes. As a model, the crystallization kinetics of warming vitreous solutions are presented here for concentrations higher than 38% (w/w) 1,3-butanediol.

Isothermal and continuous heating rate (CHR) experiments have been performed by differential scanning calorimetry and by direct optical observation using a cryomicroscope. For the isothermal method, the Johnson–Avrami equation and its second derivative were used for thermal analysis. For the CHR approach, the isoconversional method was used, assuming always a Johnson–Avrami variation for the crystallization fraction. The calorimetry results were then compared with the cryomicroscopy observations, allowing a determination of the exponent $n$. The isothermal approach gives higher calculated parameters than the CHR approach. By the isothermal approach, the Avrami exponent $n$ varies between 2.5 and 3 and the "activation energy" $E^*$ decreases from 16.9 to 11.5 kcal $mol^{-1}$. By the CHR approach, $n$ increases from 1.8 to 2.5 and the various methods used give similar results for $E^*$, with the same variations in polyalcohol concentrations as with the isothermal method. With the isothermal method, a break point is observed for both $E^*$ and $n$, determined from calorimetry, at 44–46% 1,3-butanediol. This corresponds to a change in the kinetics of the crystallization observed by cryomicroscopy.

## INTRODUCTION

A goal for long-term organ preservation at very low temperatures is to avoid ice crystallization and maintain vitrification throughout the cooling–rewarming cycle, since ice formation is the main cause of tissue injury [1,2]. Vitrification requires high concentrations of specific solutes called cryoprotectants, which must be good glass-formers and have a low

0040-6031/89/$03.50 

toxicity. Compromises must be made between the minimum concentration needed to achieve vitrification and the maximum concentration which can be tolerated by the organs. In contrast to the work of Fahy, based on dimethylsulfoxide [1,2] as a main cryoprotectant, European investigators have chosen polyalcohols as possible cryoprotectants [3,4]. Boutron and co-workers [5,6] have studied aqueous solutions of polyalcohols for their glass-forming ability on cooling, and their ability to stabilize the vitreous state during subsequent warming.

At the solute concentrations used for organ vitrification it has been found to be easier to avoid crystallization during cooling than during warming. Using red blood cells as a biological model, Boutron and co-workers have suggested that intracellular ice crystallization during warming after vitrification is not necessarily lethal [7,8]. A recent study by Takahashi et al. has shown that a correlation may exist between the size of intracellular ice crystals and the damage incurred by monocytes [9], providing a model of the injury process which is less restrictive than that of Boutron and co-workers. Boutron estimates that the warming rates needed to avoid damage during warming are approximately 600–1000 °C $min^{-1}$ [8,10], within which range the transition from cubic to hexagonal ice during warming is avoided; a transition which appears to be independent of the solute concentration. Unfortunately, the maximum warming rates currently achievable for quantitative studies do not exceed approximately 200 °C $min^{-1}$.

The objective of the present work was to quantify the amount of crystallization which occurs during warming, and correlate this with the recovery of organs after vitrification and storage. The binary system water–1,3-butanediol was chosen as a model for this kinetic study of crystallization during warming. This system is less complex than vitrification solutions previously used by Fahy, who has already achieved the vitrification of rabbit kidneys with solutions containing various cryoprotectants, each at its limit of toxicity, with different salts for the carrier solution [1]. We undertook to study a single cryoprotectant initially since, in a complex solution, each compound could have an effect on the crystallization kinetics. As a first step, we determined the parameters corresponding to isothermal or non-isothermal conditions during warming. These calculations were performed using calorimetry measurements, and the results compared to direct optical observations on a cryomicroscope.

## THEORY

### *Isothermal analysis*

For isothermal conditions, Christian has reviewed the validity of the Johnson–Avrami equation [11]

$$X = 1 - \exp(-(Kt)^n) \tag{1}$$

where $X$ is the crystallization fraction, $t$ is the time of exposure, $n$ is the Avrami exponent, and $K$ is the crystallization constant with an assumed Arrhenius variation with the temperature $T$

$$K = K_0 \exp(-E^\star/RT) \tag{2}$$

$E^\star$ being the "activation energy" and $K_0$ a constant depending on the composition. The assumption of $K$ is given to simplify the calculation even though polyalcohol solutions are known to follow the Vogel–Fulcher law [12], wherein the temperature $T$ in eqn. (2) is substituted by $T - T_0$ with $T_0$ being a characteristic temperature lower than the glass transition temperature $T_g$.

The values of the parameters $n$ and $E^\star$ can be respectively determined through plots of $\ln[-\ln(1-X)]$ vs. $\ln(t)$ and $\ln(t_{max})$ vs. $1/T$, where $t_{max}$ is the time corresponding to the maximum crystallization rate.

*Continuous heating rate analyses*

For the continuous heating rate (CHR) experiments, Henderson [13] and later Yinnon and Uhlmann [14] have reviewed the calculation methods for the determination of the various crystallization parameters in non-isothermal conditions during warming. These methods can be used with an assumed Johnson–Avrami variation for $X$. MacFarlane and co-workers have also reviewed the physical aspect of the non-isothermal kinetics for aqueous solutions [15,16], using the additive concept to develop a method of calculation as suggested by Christian [11]. Also pointed out in these studies is the importance of the theoretical approach to applications in cryopreservation by vitrification. The same approach as that of MacFarlane, has been used by other authors on systems of non-organic compounds [17,18].

For the present study, the Johnson–Avrami variation with temperature was always assumed in the CHR conditions and determination of the Avrami exponent was performed by the Ozawa method with a plot of $\ln[-\ln(1-X)]$ vs. $\ln[(T-T_0)/V]$, where $V$ is the warming rate and $T_0$ is the temperature of the beginning of the crystallization. For determination of $E^\star$ the isoconversional method was used, with an separation of the variables $X$ and $T$ in the first derivative equation deduced from eqn. (1)

$$\mathrm{d}X/\mathrm{d}T = g(X)h(T) \tag{3}$$

$$\Leftrightarrow \mathrm{d}X/g(X) = \mathrm{d}T h(T) \tag{4}$$

Three methods were used.

*(a) The Ozawa–Chen method [13]*

Considering $X$ to be constant across experiments with different warming rates, the left hand of eqn. (4) is constant after integration from 0 to $X(T)$

$$\int_{T_0}^{T} K_0 \exp(-E^\star/RT')\,\mathrm{d}T'/V = \text{constant} \tag{5}$$

Taking the approximate analytic expression of the integral due to Doyle [13] as given here,

$$\ln(K_0 R/E^\star) + \ln(T^2/V) - E^\star/RT = \text{constant} \tag{6}$$

*(b) The Flynn method [19]*

Similar to the previous development, this method uses a numerical expression of the integral of eqn. (5), giving

$$\ln(K_0 E^\star/R) + \ln(V) + 1.052 E^\star/RT = \text{constant} \tag{7}$$

This calculation has also been done by Kemény and Gránásy [20]. In the present work, the corrections suggested by Flynn [19] have not been used.

*(c) The Augis–Bennett method [13]*

This method starts from the first derivative of the Johnson–Avrami equation using the second derivative to determine the particular conditions for the maximum crystallization rates with $d^2X/dT^2 = 0$ and $T = T_d$ corresponding to the bottom of the devitrification peak for the DSC measurements. Assuming $E^\star/RT_d \gg 1$, they have shown

$$[K_0(T_d - T_0)\exp(-E^\star/RT_d)]/V = \text{constant} \tag{8}$$

## MEASUREMENTS

1,3-Butanediol ("99%") from Aldrich, mixed with dcionized water, was used for all the sample solutions. All concentrations are expressed in per cent by weight.

Concentrations of 38–46% of 1,3-butanediol were used in order to achieve vitrification of the solution on cooling [5]. Calorimetry experiments were performed using a Perkin–Elmer DSC-4, either in the scanning mode (for the CHR experiments) or using the Isothermal Software Kit (for the isothermal experiments). All samples were cooled to $-140\,^\circ$C at $200\,^\circ$C min$^{-1}$, warmed at $200\,^\circ$C min$^{-1}$, and maintained at the chosen temperatures for the isothermal experiments. Warming rates of 3–80 °C min$^{-1}$ were used for the CHR experiments.

The same solutions were used for direct observations of the crystallization on a cryomicroscope (Zeiss Jena Pereval "Interphako" interferometric microscope) with a temperature-programmable cold stage (Linkam). Ice crystallization is recorded on video tape and observed on a TV screen with a sample-to-screen magnification of 500 ×. This system only achieves cooling rates up to $20\,^\circ$C min$^{-1}$, which is not sufficient to achieve complete vitrification of the solution. Therefore, samples placed between two circular glass covers were directly quenched into liquid nitrogen and then placed in

the cryomicroscope precooled to $-140\,^{\circ}C$. Both isothermal and CHR experiments were performed with the cryomicroscope. The warming rates used were $50\,^{\circ}C\ min^{-1}$ for the isothermal experiments and $10–40\,^{\circ}C\ min^{-1}$ for the CHR experiments.

## RESULTS

### *Optical observations and calorimetry*

#### *Crack formation*

Figure 1 shows DSC-4 measurements compared with direct observations with the cryomicroscope. In general, cracks occurred during quenching, because of the rapid cooling rates and the large thermal gradients below the glass transition. This has also been observed by Williams and Carnahan for aqueous solutions of sucrose [21] and hydroxyethylstarch solutions (personal communication). During the warming of 44% 1,3-butanediol, cracks are seen to disappear, presumably by molecular diffusion or by relaxation from the glassy state to the supercooled liquid at temperatures close to the glass transition (Fig. 1). At higher temperatures these fractures reappear with bubble formation or nucleation and crystallization. Bubble formation did

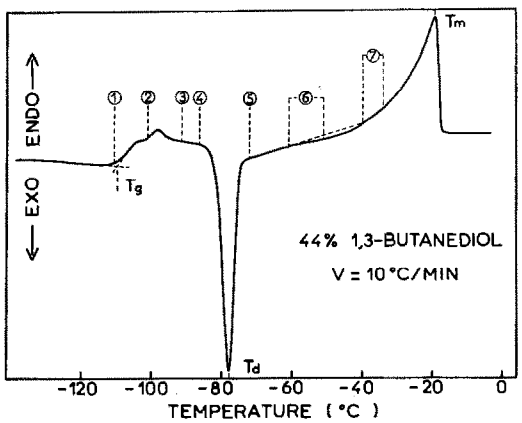


Fig. 1. Comparison of cryomicroscopy and DSC observations on 44% 1,3-butanediol with water. Samples were quenched directly in liquid nitrogen and then placed in the cryomicroscope at $-140\,^{\circ}C$; or "quenched" at $200\,^{\circ}C\ min^{-1}$ to $-140\,^{\circ}C$ in the DSC. Cracks were observed with the cryomicroscope after the quenching in liquid nitrogen. Both samples were warmed back to $0\,^{\circ}C$ at $10\,^{\circ}C\ min^{-1}$. (1) Beginning of the disappearance of the cracks by relaxation; (2) end of the disappearance of the cracks; (3) reappearance of cracks by bubble formation or nucleation and crystal growth; (4) beginning of crystallization in the bulk solution; (5) end of crystallization; (6) beginning of a darkening effect in the solution; (7) end of the darkening effect. ($T_g$ = glass transition temperature, $T_d$ = devitrification temperature, $T_m$ = temperature at the end of melting.)

not preclude nucleation and crystallization nor did it increase the nucleation or crystallization rate when cracks with or without bubbles were compared. Fractures were seen to act as "heterogeneous" sites for nucleation. A discussion of the nature of this nucleation effect has been provided by Williams and Carnahan [21]. Presumably local stresses along the cracks can change the local order in the glassy matrix.

*Nucleation, crystal growth and devitrification*

In the DSC in the absence of cracks, bulk solution nucleation and crystal growth occurred at temperatures the same as or higher than for the direct observations in the absence of cracks, or between cracks by cryomicroscopy as seen in Fig. 1. This accord between the observations and the measurements disappeared with increasing concentrations higher than 44% 1,3-butanediol.

*Darkening effect*

A darkening effect was also observed at higher temperatures, corresponding to a weak exothermal peak before the melting peak (Fig. 1). Generally this effect is observed macroscopically at the same time as the devitrification peak for concentrated aqueous solutions [22], but in this instance the effect occurred at higher temperatures than the temperature of devitrification $T_d$. This effect, therefore, is subsequent to crystallization on warming. We have observed an apparent "homogeneization" of the medium just before the beginning of the darkening process. Indeed, in the medium containing different large crystals, dislocation borders between crystals can be seen to disappear. After "homogeneization", different kinds of compact crystal seem to grow, appearing more or less dark and with a very small size compared to crystals at the completion of devitrification. This is particularly true for the highest concentrations, where the low nucleation density allows the crystals to grow to large sizes. This darkening effect for the binary system looks like a restructuring of the crystals rather than a recrystallization by an "Ostwald ripening". Indeed, this last theory argues that the larger crystals grow and the smaller ones decrease in size, suggesting melting of the smaller crystals in favour of the larger ones, with an exchange of endo–exothermal energies during the local diffusional processes. The present observations are not sufficient to allow analysis of the mechanism of the darkening effect. However, the cracks are also seen to disappear during or just after the glass transition and subsequently to reappear as a result of nucleation/crystallization even during the darkening effect. Moreover, the crystals associated with these cracks are among the last crystals to melt on warming. This darkening effect could be interpreted as a relaxation phenomenon after the explosive crystallization inside the medium during devitrification, segregating highly concentrated supercooled liquid trapped between crystal fronts.

*Quantitative observations of nucleation and crystal growth*

We examined crystal growth at various solute concentrations. At low concentrations the crystallization process is rapid, with a very large number of nuclei and an apparently broad crystal size distribution, as compared to 44% concentration, in which all of the crystals are the same size. At 44%, the observable crystals are spherical, as has been previously reported for other concentrated aqueous solutions [23–25]. Where a spatially isotropic crystallization is observed, the nature of the nucleation is mostly homogeneous. With increasing concentration the nucleation density decreases, and some of the crystals are seen to grow from a defect or impurity present in the solution, which means that the nucleation also becomes more heterogeneous with increasing concentration. Assuming that these spherulites are compact, the Avrami exponent can be determined (see Appendix). In Fig. 2 the log of the crystal diameter $D$ is plotted as a function of the log of time $\Delta t$ with isothermal conditions at various temperatures. The time of induction for the formation of the nuclei was not taken into account in determining $t$. A linear variation is observed in Fig. 2.

A preliminary statistical enumeration of the visible crystals inside the medium as a function of the heating rate for 46% 1,3-butanediol showed that the nucleation density seems to be proportional to $V^{-a}$, where $V$ is the warming rate and $a$ is an exponent varying between 0.5 and 1.7 for this concentration. The fewer nuclei that form, the higher the temperature of the devitrification peak corresponding to the maximum crystallization rates, the lower the values of the activation energy $E^{\star}$, and the slower the crystallization rate. From cryomicroscopy samples prepared by quenching in liquid nitrogen, it appears that the nucleation density is proportional to the time allowed during warming for the initiation of nuclei. There is also an

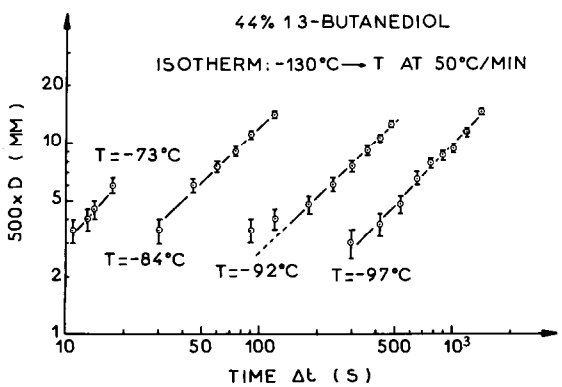


Fig. 2. Isothermal crystallization in 44% 1,3-butanediol with the cryomicroscope at different temperatures. Spherulite crystals were observed and their diameter $D$ plotted as a function of the time $\Delta t$ of exposure at the respective temperatures. Both $D$ and $\Delta t$ are reported on logarithmic scales. For the time $\Delta t$, the induction time for nucleation is not considered.

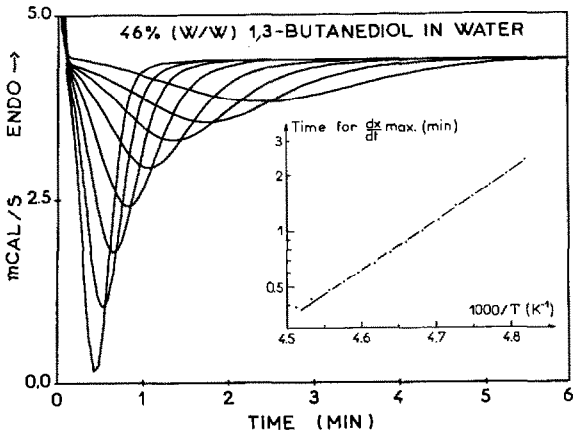


Fig. 3. DSC isothermal crystallization peaks as a function of the time of exposure at different temperatures for 46% 1,3-butanediol in water. The inset figure shows a plot of the time $t_{max}$ corresponding to the maximum crystallization rate as a function of $1000/T$ for the same isothermal crystallization peaks.

apparent dependence on the relaxation time to permit molecular diffusion in the highly supercooled liquid above the glass transition.

*Calorimetry experiments*

The isothermal crystallization peaks for 46% 1,3-butanediol are presented in Fig. 3 for various temperatures, $T$, as a function of exposure time: $\ln(t_{max})$ is plotted as a function of $1000/T$. The slope is proportional to $E^{\star}$

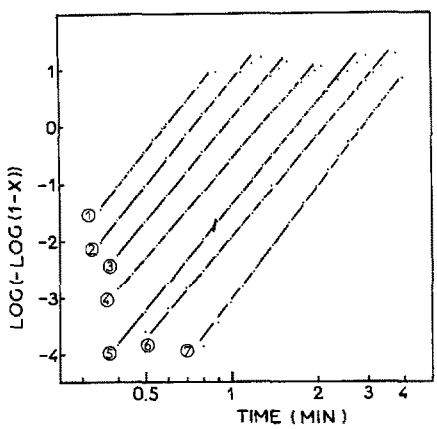


Fig. 4. Plot of $\ln(-\ln(1-X))$ as a function of the time of exposure for the same sample as shown in Fig. 3. Each line corresponds to a single isothermal crystallization peak, and $X$ is the crystallization fraction. (1) $T = 218.6$ K; (2) $T = 216.6$ K; (3) $T = 214.6$ K; (4) $T = 212.6$ K; (5) $T = 210.6$ K; (6) $T = 208.6$ K; (7) $T = 206.6$ K.

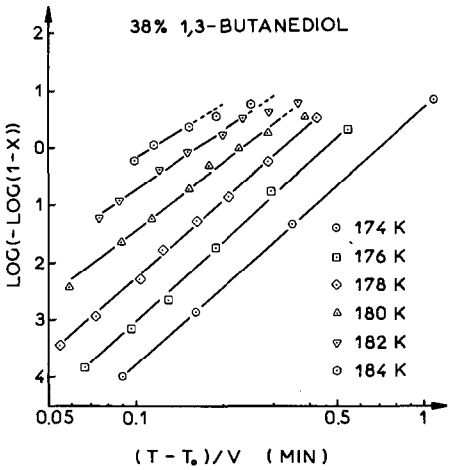


Fig. 5. Ozawa plot of $\ln[-\ln(1-X)]$ as a function of $(T-T_0)/V$ for 38% 1,3-butanediol at different constant temperatures. $T_0$ is the temperature of the beginning of crystallization, and $V$ is the warming rate.

(see Theory). In Fig. 4, $\ln[-\ln(1-X)]$ is plotted as a function $\ln(t)$ for the same peaks, where the slopes of the lines are proportional to $n$ (see Theory).

For the CHR experiments, a linear baseline is assumed in which the solute–solvent heat of mixing and the thermal variation of heat of crystallization are ignored. This last correction is negligible in the temperature range

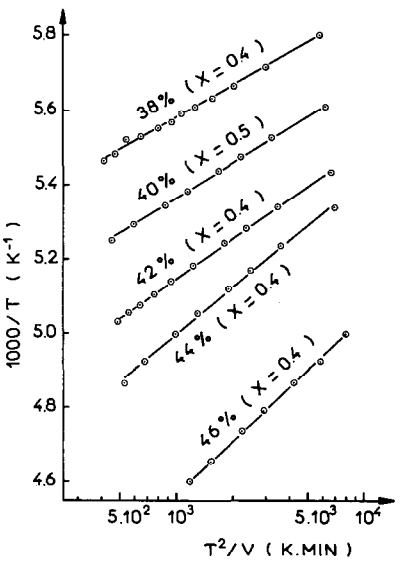


Fig. 6. Ozawa–Chen plot of $1000/T$ as a function of $T^2/V$ on a logarithmic scale for different concentrations of 1,3-butanediol, maintaining the crystallization fraction $X$ constant for different CHR experiments at different warming rates $V$.

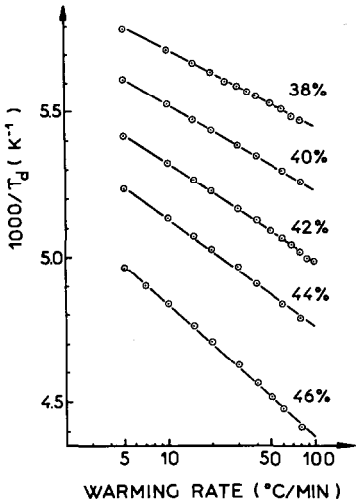


Fig. 7. Flynn plot of $1000/T_d$ as a function of $V$ on a logarithmic scale for different concentrations of 1,3-butanediol, where $T_d$ is the devitrification temperature defined in Fig. 1.

we used, as has been demonstrated by Mikhalev et al. [26]. The Ozawa plot shown in Fig. 5 for 46% 1,3-butanediol allows the determination of $n$. For the determination of $E^*$, Figs. 6–8 show, respectively, the Ozawa–Chen

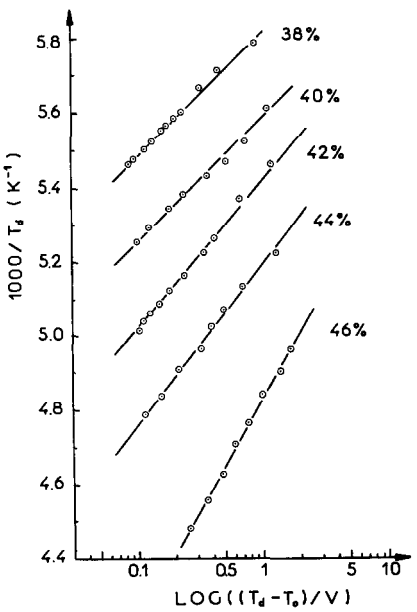


Fig. 8. Augis–Bennett plot of $1000/T_d$ as a function of $(T_d - T_0)/V$ on a logarithmic scale for different concentrations of 1,3-butanediol. The notation is as for Figs. 5 and 7.

TABLE 1

Avrami exponent $n$ for different concentrations of 1,3-butanediol with water for isothermal and continuous heating rate (CHR) experiments from DSC and cryomicroscopy [a,b]

| | | 1,3-But(OH)$_2$ concentration (% w/w) | | | | |
|---|---|---|---|---|---|---|
| | | 38 | 40 | 42 | 44 | 46 |
| DSC | Isothermal | 2.59 [0.26] | 2.66 [0.24] | 3.04 [0.35] | 3.02 [0.06] | 2.63 [0.16] |
| | CHR | 1.77 [0.22] | 1.79 [0.07] | 2.08 [0.15] | 2.14 [0.07] | 2.42 [0.14] |
| Cryomicroscopy [c] | Isothermal | Non-obs. | Non-obs. | Non-obs. | 2.75 [0.34] | 2.52 [0.40] |
| | CHR | Non-obs. | Non-obs. | Non-obs. | Non-obs. | 3.82 [0.07] |

[a] The values are the mean values calculated from the determinations by a linear regression of the first order by approximation of the least square. The values of the variance $\sigma$ are given in parentheses.

[b] The values of the CHR experiments are much lower than the other values. This could be due to the choice of the initial temperatures $T_0$ for the different CHR analyses. The value of $\sigma$ does not take into account the approximation of the linear basal line for the devitrification peaks.

[c] Non-obs.: the value of $n$ was not determined. Either crystal growth was too rapid, or the number of nuclei was too high.

plot, the Flynn plot and the Augis–Bennett plot for different concentrations of 1,3-butanediol. A good linear variation for these different plots is observed.

All slopes of the various lines drawn for the determination of $n$ and $E^\star$ were calculated by a least-squares linear regression with a correlation coefficient higher than 0.990. For $n$ the mean values and variances were determined for the different peaks used for the calculations. Values of the exponent $n$ and $E^\star$ are reported in Tables 1 and 2, respectively. Table 1 reports the results of direct calculation of the exponent $n$ with the cryomicroscope. The energy (Table 2) for the isothermal calorimetry de-

TABLE 2

Comparison of activation energy values obtained by isothermal and CHR experiments for different concentrations of 1,3-butanediol from DSC [a]

| 1,3-But(OH)$_2$ concentration (% w/w) | Isothermal (kcal mol$^{-1}$) | CHR (kcal mol$^{-1}$) | | |
|---|---|---|---|---|
| | JAM equation | Ozawa–Chen | Flynn | Augis–Bennett |
| 38 | 16.9 | 14.9–15.8 | 16.1 | 13.5 |
| 40 | 16.3 | 14.3–14.7 | 14.5 | 14.2 |
| 42 | 16.0 | 12.5–12.8 | 13.1 | 12.4 |
| 44 | 15.6 | 10.8–11.1 | 11.6 | 10.5 |
| 46 | 11.9 | 9.6– 9.8 | 9.5 | 7.8 |

[a] Determination of the activation energy $E^\star$ was done by linear regression with a least-squares approximation giving a correlation factor of less than 0.990.

creases with increasing concentration. This decrease is linear from 16.9 to 15.6 kcal $mol^{-1}$ and drops more rapidly to 11.9 kcal $mol^{-1}$ for 46% 1,3-butanediol. The CHR experiments for the three methods give lower values of $E^{\star}$ than the isothermal experiments. However, the three methods give generally similar results and the same variations with concentration as obtained from the isothermal measurements. In Table 1, the values of $n$ increase with concentration from 2.5 to 3 up to 44% 1,3-butanediol under isothermal conditions, and then decrease to 2.5 for 46%. For the CHR experiments, the values are much lower and increase gradually with concentration from 1.8 to 2.4. For the direct observations with the cryomicroscope the isothermal values of $n$ are consistent with those calculated from the calorimetry experiments. For the CHR experiments, the only value for 46% is higher than the one calculated by the DSC approach.

## DISCUSSION

### *Isothermal experiments*

#### *Avrami exponent*

Comparing the results for the value of the Avrami exponent $n$ obtained by calorimetry and by cryomicroscopy, we note that the value of $n = 3$ for 44% 1,3-butanediol is consistent with the theory reported by Christian for a constant nucleation density during crystal growth and for an interface-controlled growth for a growth dimension of 3 [11]. For concentrations lower than 42% the value of $n$ is smaller, probably as a result of a change in the crystallization kinetics: the nucleation density might increase steadily with time, converging to values around 2.5 for the exponent $n$. The thermal range of nucleation may be wider, and it overlaps the crystal growth domain. The maximum crystal size is small and the space between crystals is smaller. An explanation for these exponents $n$ might lie in the initial stage of growth by diffusion generally observed as in Fig. 2 for the higher concentrations for isothermal measurements, as suggested by the theoretical exponent specified by Christian [11].

For concentrations of 44 and 46%, the values determined directly from the optical observations reported in Table 1 are in good agreement with those calculated from the calorimetric experiments.

#### *Activation energy*

The linear variation of the activation energy $E^{\star}$ for concentrations of 38–44% in Table 2 is not in disagreement with the previous hypothesis concerning the values of the exponent $n$, considering that the determination of these energies is done at the maximal crystallization rates for different temperatures. Moreover, the decrease of the activation energy $E^{\star}$ shows the

relative stability of the wholly vitreous state during the rewarming. It has already been reported by Zhao and Sakka for glasses containing LiF [18] that maximum glass-forming ability corresponds to a minimum of activation energy.

The break point between 44 and 46% for $E^*$ shows a transition for the stability of the vitreous state corresponding to a change in the crystallization process. First, for concentrations of 46% or higher under CHR conditions, the spherulites show an evanescent nature with dendritic form growing from the surface for critical size. This effect could be temperature dependent [23–25]. The lower density of nuclei is probably responsible for the fact that the crystals grow to larger sizes. This break point is also observed for the exponent $n$ in Table 1 but with less magnitude. However, for the isothermal experiments, the direct observations of the crystals at 44% do not exhibit any evanescent processes, nor do they at 46% for temperatures lower than $-70\,^{\circ}\mathrm{C}$. Moreover, the fact that the density of nuclei may be lower in the DSC experiments than with cryomicroscopy may allow larger spherulites for the DSC experiments. The evanescent nature of the crystal may also be hidden owing to the insensitivity of the apparatus.

*CHR experiments*

Considering the results in Tables 1 and 2, the calculated values for the CHR experiments are consistent across the three methods for the determination of $E^*$, as are the variations of $E^*$ and $n$ with 1,3-butanediol concentration for the isothermal and CHR experiments. However, the CHR values are lower than the isothermal values. For the CHR experiments, the warming rates used are up to $80\,^{\circ}\mathrm{C\ min^{-1}}$, as compared with $200\,^{\circ}\mathrm{C\ min^{-1}}$ for the isothermal experiments. The nucleation density must be higher in the CHR experiments, and the crystallization could stay at its early stage. This increase in density does not explain the values determined for $n$. The values given by Christian [11] for isothermal conditions are then not well defined, especially if the constant $K_0$ is dependent on the nucleation rate, which is itself dependent on the rate of warming. Assuming a nucleation density proportional to $V^{-a}$ for the present study, the Ozawa plot must be corrected by drawing $\ln(-\ln(1-X))$ as a family of curves as a function of $\ln((T-T_0)/V^{1+a})$ for different experiments at different warming rates and for chosen temperatures with eqn. (2) as the expression for the crystallization constant. The problem then is to determine the average value of $a$ as a function of warming rate. The correction depends upon the observations made with the cryomicroscope in order to relate the exponent $a$ to the warming rate $V$. This part of the calculation has not yet been performed for this solution and will be presented in a later paper. This consideration will probably lower the value of the Avrami exponent, as has been shown by MacFarlane and co-workers [15,16], and increase the discrepancy between

the values of $n$ determined by the isothermal and CHR methods. This discrepancy might also come from the choice of the initial temperature $T_0$: the lower the value of $T_0$, the higher the value of $n$. The choice of the linear baseline can induce a variation of the crystallization fraction, by taking twice the logarithm of $(1 - X)^{-1}$, and a variation of the determination of $n$. The variation of $n$ with the choice of $T_0$ is more sensitive. Indeed, if $T_0 = 0$ K then the Ozawa plot gives values of $n$ from around 3.5 to 4.5 for the different concentrations.

It should also be noted that for the CHR measurements, the break point between 44 and 46% is less apparent than for the isothermal experiments for the exponent $n$ and the activation energy $E^\star$.

## CONCLUSIONS

The isothermal experiments are useful for understanding the mechanism of crystallization on warming of the vitreous state using the complementary techniques of DSC and cryomicroscopy. The CHR experiments show that determination of these parameters by calorimetry generally confirms the isothermal information on the kinetics of crystallization. These CHR parameters alone do not suffice, as it has been shown that the Ozawa method is not especially accurate for the determination of $n$. However, the variation obtained for this exponent and for $E^\star$ may allow extrapolation to higher concentrations if the calculations use the same methods. By these extrapolations an estimation, however inaccurate, of the crystallization fraction is available for high concentrations of solutes. These techniques are commonly used for similar studies of devitrification in metallic or non-organic glasses at relatively high temperatures. This study also shows that ice crystallization in even such a simple binary system as this is already complex, though more different kinds of ice crystals have been observed in other concentrated aqueous solutions [23–25].

The damage which might occur to vitrified organs during warming has to be correlated to the size of the crystals, their shape, and also the amount of crystallization taking place. The combination of calorimetry and cryomicroscopy allows such studies. We intend to follow the present work with a study extrapolating these results to 1,3-butanediol concentrations of 48% and higher, to determine the amount of crystallization before the melting process, and to compare these with the experimental results.

A phenomenon crucial to the development of the cryopreservation of organs by vitrification is crack formation. It is important to understand how crack formation is initiated. Indeed, the presence of microfractures can produce an excess of crystallization during the warming stage of the organs, extending the amount of damage. The combination of calorimetry and cryomicroscopy could be a good tool to investigate this process.

The theory developed by Boutron on the non-equilibrium ice crystallization in aqueous solutions of polyalcohols [27] is not used here but will be related to these results in a subsequent paper.

## APPENDIX

### *Determination of the exponent n by direct optical observation*

In our case the observed crystals look like spherulites and are assumed to be spherical with an isotropic crystal growth. We assume that the crystals do not grow on the top of the cover glass as a cone. By assuming that the nucleus forms inside the bulk solution we determine the rate of radial growth. A plot is made of $\log(D)$ vs. $\log(\Delta t)$, where $D$ is the diameter of the crystal after a time $\Delta t$ corresponding to the time during which the crystal grows actively. A linear relation between these two logarithms then gives a relation between $D$ and $\Delta t$

$$D = D_0(\Delta t)^m \tag{A.1}$$

The volume of the crystal is

$$V(\Delta t) = \pi D_0^3(\Delta t)^{3m}/6 \tag{A.2}$$

Then for a number $N$ of nuclei formed under conditions of site saturation, the crystallization fraction has the same definition as that used by Christian [11]

$$X(\Delta t) = 1 - \exp\{-[NV(\Delta t)/V_0]\} \tag{A.3}$$

where $V_0$ is the crystallizable volume of the solution. Substituting $V(\Delta t)$ from eqn. (A.2) into eqn. (A.3), we obtain

$$X(\Delta t) = 1 - \exp\left\{-\left[\left(N\pi D_0^3/6V_0\right)(\Delta t)\right]^{3m}\right\} \tag{A.4}$$

This is an expression similar to that of Johnson–Avrami with an exponent $n = 3m$. In practice, in this study, the growth is not considered after the contact between crystals for the determination of the diameter $D$. As mentioned in the text, the nucleation density can be dependent on the warming rate, particularly for the CHR experiments. However, this direct calculation from the observations does not take into account the number of nuclei for the determination of the exponent $n$, even if $N$ might be dependent on the warming rate. The same calculation can be done for a growth in two dimensions which gives $n = 2m$, or in one dimension with $n = m$ if the dimension corresponding to the slower growth is assumed constant during the measurements.

ACKNOWLEDGEMENTS

The author is grateful to H.T. Meryman for his support of this study and R.J. Williams and A. Hirsh for their suggestions, experimental help and revision of the manuscript, G.M. Fahy for his support, and D. Carnahan for his technical assistance. Thanks are also due to Joanne G. Brass for her assistance with the elaboration of this manuscript. The work was supported by grant BSRG 2 S07RR05737 and NIH grant 5R01GM-17959-15.

REFERENCES

1 G.M. Fahy, D.R. MacFarlane, C.A. Angell and H.T. Meryman, Cryobiology, 21 (1984) 407.
2 G.M. Fahy, in J.J. MacGrath and K.R. Diller (Eds.), Low Temperature Biotechnology: Emerging Applications and Engineering Contributions, BED-Vol 10/HTD-Vol 98; The American Society of Mechanical Engineers, New York, 1988, pp. 113–148.
3 D.E. Pegg, I.B. Jacobsen, M.P. Diaper and J. Foreman, Cryobiology, 24 (1987) 420.
4 I.B. Jacobsen, in D.E. Pegg and A.M. Karow, Jr., (Eds.), The Biophysics of Organ Cryopreservation, Plenum Press, London, 1988, pp. 15–21.
5 P. Boutron, P. Mehl, A. Kaufmann and P. Angibaud, Cryobiology, 23 (1986) 453.
6 P. Boutron and P. Mehl, J. Phys. (Paris), Coll. Cl, Suppl. 3, 48 (1987) 441.
7 P. Boutron and F. Arnaud, Cryobiology, 21 (1984) 348.
8 P. Mehl and P. Boutron, Cryobiology, 25 (1988) 44.
9 T. Takahashi, A. Hirsh, E. Erbe and R.J. Williams, Biophys. J., 54 (1988) 509.
10 P. Boutron, in D.E. Pegg and A.M. Karow, Jr., (Eds.), The Biophysics of Organ Cryopreservation, Plenum Press, London, 1988, pp. 201–228.
11 J.W. Christian, in R.W. Cahn (Ed.), Physical Metallurgy, North Holland, Amsterdam, 1965, pp. 443–539.
12 C.A. Angell, in K.L. Ngai and G.B. Wright (Eds.), Relaxations in Complex Systems, National Technical Information Service, U.S. Department of Commerce, Springfield, Va. (U.S.A.), 1988, pp. 3–11.
13 D.W. Henderson, J. Non-Crystal. Solids, 30 (1979) 301.
14 H. Yinnon and D.R. Uhlmann, J. Non-Crystal. Solids, 54 (1983) 253.
15 D.R. MacFarlane, M. Mateki and M. Poulain, Cryobiology, 23 (1986) 230.
16 D.R. MacFarlane and M. Forsyth, in D.E. Pegg and A.M. Karow, Jr., (Eds.), The Biophysics of Organ Cryopreservation, Plenum Press, London, 1988, pp. 237–257.
17 K. Matusita, K. Miura and T. Komatsu, Thermochim. Acta, 88 (1985) 283.
18 X. Zhao and S. Sakka, J. Non-Crystal. Solids, 95–96 (1987) 487–494.
19 J.H. Flynn, Proc. XIIth NATAS Conf., September, 1983, Paper 125.
20 T. Kemény and L. Gránásy, J. Non-Crystal. Solids, 68 (1984) 193.
21 R.J. Williams and D. Carnahan, Thermochim. Acta, 155 (1989) 103.
22 M. Forsyth and D.R. MacFarlane, Cryo-Letters, 7 (1986) 367.
23 B. Luyet, Biodynamica, 10 (1969) 277.
24 G. Rapatz and B. Luyet, Biodynamica, 10 (1969) 69.
25 B. Luyet and G. Rapatz, Biodynamica, 10 (1969) 293.
26 O.I. Mikhalev, A.T. Kaplan and V.I. Trofinov, Chem. Phys. Lett., 21 (1985) 547.
27 P. Boutron, Cryobiology, 23 (1986) 88.